

WISE TF: A MID-INFRARED, 3.4 μm EXTENSION OF THE TULLY-FISHER RELATION USING WISE PHOTOMETRY

DAVID J. LAGATTUTA^{1,2}, JEREMY R. MOULD^{1,2}, LISTER STAVELEY-SMITH^{2,3}, TAO HONG^{2,3,4}, CHRISTOPHER M. SPRINGOB^{2,3,5}, KAREN L. MASTERS^{6,7}, BÄRBEL S. KORIBALSKI⁸, AND D. HEATH JONES⁹

Accepted to The Astrophysical Journal: 9 May 2013

ABSTRACT

We present a mid-infrared Tully-Fisher (TF) relation using photometry from the 3.4 μm *W1* band of the *Wide-field Infrared Survey Explorer* (*WISE*) satellite. The *WISE* TF relation is formed from 568 galaxies taken from the all-sky 2MASS Tully-Fisher (2MTF) galaxy catalog, spanning a range of environments including field, group, and cluster galaxies. This constitutes the largest mid-infrared TF relation constructed, to date. After applying a number of corrections to galaxy magnitudes and line widths, we measure a master TF relation given by $M_{\text{corr}} = -22.24 - 10.05[\log(W_{\text{corr}}) - 2.5]$, with an average dispersion of $\sigma_{\text{WISE}} = 0.686$ magnitudes. There is some tension between *WISE* TF and a preliminary 3.6 μm relation, which has a shallower slope and almost no intrinsic dispersion. However, our results agree well with a more recent relation constructed from a large sample of cluster galaxies. We additionally compare *WISE* TF to the near-infrared 2MTF template relations, finding a good agreement between the TF parameters and total dispersions of *WISE* TF and the 2MTF K-band template. This fact, coupled with typical galaxy colors of $(K - W1) \sim 0$, suggests that these two bands are tracing similar stellar populations, including the older, centrally-located stars in the galactic bulge which can (for galaxies with a prominent bulge) dominate the light profile.

Keywords: distance scale — galaxies: fundamental parameters — galaxies: spiral — infrared: galaxies

1. INTRODUCTION

Scaling relationships play an important role in understanding the nature and behavior of galaxies. This is because it is often possible to infer properties that are difficult to measure (such as stellar age) from other, more readily available information (such as metallicity fraction). While there are a number of scaling relations currently in use in modern astronomy, such as the Faber-Jackson law (Faber & Jackson 1976), the $D_n - \sigma$ relationship (Dressler 1987), the fundamental plane (Dressler et al. 1987; Djorgovski & Davis 1987), and the bulge black hole mass relation (Ferrarese & Merritt 2000), rotationally dominated (i.e., spiral) galaxies can be described by the Tully-Fisher (TF) relation. First measured by Tully & Fisher (1977), the TF relation measures the correlation between a galaxy's total luminos-

ity and maximum rotational velocity, finding that the brighter a galaxy is, the faster it rotates, leading to wider measured rotation curves.

Originally, the TF relation was measured using B-band luminosities (Tully & Fisher 1977), but a large dispersion around the fitted slope (due primarily to dust extinction, scattering, and galactic attenuation) somewhat limited its utility. Later speculations suggested that longer-wavelength data, being less susceptible to extinction and recent star formation, would show a smaller dispersion (Aaronson et al. 1979), and this prompted the creation of TF relations in redder bands. In particular, there have been several TF relations constructed in both the optical (e.g., Bothun & Mould 1987; Giovanelli et al. 1997; Tully & Pierce 2000; Verheijen 2001; Masters et al. 2006; Mocz et al. 2012) and the near-infrared (e.g., Aaronson et al. 1980; Bernstein et al. 1994; Rothberg et al. 2000; Macri 2001; Masters et al. 2008; Theureau et al. 2007). While the specific TF parameters (slope and intercept of a linear fit) vary from study to study, the TF scatter does generally decrease as the observed wavelength increases.

In this work, we continue to extend the redward trend of TF relations, using luminosity data obtained from the *Wide-field Infrared Survey Explorer* (*WISE*; Wright et al. 2010) satellite. Like the previous 2-Micron All Sky Survey (2MASS; Skrutskie et al. 2006), the *WISE* mission was designed to image the entire sky in the IR regime. However, *WISE* is equipped with much redder bandpass filters (3.4, 4.6, 12, and 22 μm), making it a mid-infrared (mid-IR) instrument.

At the very longest mid-IR wavelengths, photons from warm dust and gas dominate galaxy luminosity, rather than direct stellar emission. Due to the spatially variable nature of dust in galaxies, TF relations constructed

dlagattu@astro.swin.edu.au

¹ Centre for Astrophysics & Supercomputing, Swinburne University of Technology, P.O. Box 218, Hawthorn, VIC 3122, Australia

² ARC Centre of Excellence for All-sky Astrophysics (CAASTRO)

³ International Centre for Radio Astronomy Research (ICRAR), University of Western Australia, 35 Stirling Highway, Crawley, WA 6009, Australia

⁴ National Astronomical Observatories, Chinese Academy of Sciences, 20A Datun Road, Chaoyang District, Beijing 100012, China

⁵ Australia Astronomical Observatory, PO Box 915, North Ryde, NSW 1670, Australia

⁶ Institute for Cosmology and Gravitation, University of Portsmouth, Dennis Sciama Building, Burnaby Road, Portsmouth, PO1 3FX, UK

⁷ South East Physics Network, www.sepnet.ac.uk

⁸ CSIRO Astronomy and Space Science, Australia Telescope National Facility (ATNF) PO Box 76, Epping, NSW 1710, Australia

⁹ School of Physics, Monash University, Clayton, VIC 3800, Australia

at these wavelengths may show significantly increased scatter, as the empirical relationship (originally designed to match stellar luminosity and rotation) is altered by this extra flux. In order to avoid this possibility, we only focus on the shortest *WISE* bandpass (3.4 μm), where, after fitting a 300 K blackbody spectrum to the mid-IR spectral energy distribution of a typical star forming galaxy (e.g., Zheng et al. 2007), we find that only 1% to 5% of the total emission at 3.4 μm is due to dust.

By utilizing 3.4 μm data, we are able to compare our results to the surprising 3.6 μm TF relation presented in Freedman & Madore (2010). In that work, a mid-IR TF relation was constructed from a sample of eight galaxies cross-matched between the *Hubble Space Telescope* Key Project’s Cepheid distance sample (Sakai et al. 2000) and a catalog of nearby galaxies (Dale et al. 2007) imaged with the *Spitzer Space Telescope*. (Two of these galaxies, NGC 4725 and NGC 7331, are included in our final data set.) Without explicitly correcting for several systematic effects, the sample showed a remarkably small dispersion ($\sigma \sim 0.12$ mags), opening up the possibility that the mid-IR TF relation could be used as a tool for measuring precision cosmological and distance parameters. However, as correctly noted in that paper, a much larger sample of galaxies – preferably containing objects with more commonly observed magnitudes – is needed to verify (or reject) this result. Using data acquired from an all-sky instrument such as *WISE*, we are in a prime position to attempt such a task.

This paper, along with the preliminary work by Freedman & Madore (2010) and the work of Sorce et al. (2012a,b, 2013), presents the first TF relationship constructed at mid-infrared wavelengths, and allows us to probe some empirical properties of galaxies in a regime where the oldest (assuming inside-out growth of stellar mass; e.g., Pérez et al. 2013), most centrally-located stars make up a slightly more prominent fraction of the total luminosity (Buta et al. 2010). In addition to galaxy properties, however, the TF relation can also be used for cosmological purposes. Specifically, the TF relation can be used to measure peculiar velocities, which can, when taken over a large enough volume, begin to constrain the dark matter distribution in the Local Universe. With a potentially lower TF scatter in the mid-IR, peculiar velocities can be more robustly determined, ultimately resulting in better dark matter mapping and an improved understanding of the nature of the Universe’s mass structure.

This paper is organized as follows: In Section 2 we describe the data products (magnitudes and line widths) used in this work, along with the initial catalog and specific data cuts used to construct the final galaxy sample. In Section 3, we outline our TF analysis, highlighting several corrections designed to homogenize the galaxy sample. It is in this section where we present the final, best-fit *WISE* TF relation. We discuss the results of the TF analysis in Section 4. Specifically, we compare the parameters of *WISE* TF to other near- and mid-IR TF relations and identify potential sources of intrinsic TF scatter at mid-IR wavelengths. We briefly conclude in Section 5. Additionally, technical details testing the accuracy of the peculiar velocity corrections, along with measurements showing the effects of the corrections on the final TF relation, are presented in an Appendix.

Throughout this work, we assume a Hubble parameter $H_0 = 100 h \text{ km s}^{-1} \text{ Mpc}^{-1}$. All magnitudes are calculated in the Vega system.

2. DATA

We select the initial TF candidate galaxies by cross-matching magnitudes from the *WISE* *W1* (3.4 micron) all-sky data release catalog with rotational velocity (H I line width) measurements from the 2MASS Tully Fisher (2MTF; Masters et al. 2008) all-sky galaxy catalog (Masters et al. 2008; Hong et al. 2013). While the complete 2MTF catalog contains line width measurements acquired from archival sources – the Cornell H I digital archive (Springob et al. 2005) and the HYPERLEDA database (Theureau et al. 1998, 2005; Paturel et al. 2003) – and new observational data from the Green Bank Telescope and the Parks Radio Telescope (Hong et al. 2013), we construct the *WISE* TF relation using only the publicly available line width data (i.e., the Cornell and HYPERLEDA samples). Although there are selection effects embedded in the overall archival catalogs (due to the heterogeneous nature of how they were compiled), the subset of the data comprising the 2MTF sample is specifically designed to be complete down to magnitude $K = 11.5$, minimizing any potential selection bias. We explicitly exclude galaxies in a related catalog, the 2MTF “galaxy template” sample (Masters et al. 2008) from our final data set, as this sample will be analyzed separately in a companion paper. Because the remaining “non-template” 2MTF galaxies cover a larger area of the sky, include a wider range of environments (from clusters, to groups, to field galaxies), and span a similar redshift range ($0 < z < 0.05$), removing the galaxy template sample from our analysis will not bias the final results.

In the *WISE* catalog, magnitudes of resolved 2MASS galaxies are measured using an elliptical aperture designed to mimic the size and shape of a given galaxy. This is achieved by convolving the galaxy’s shape, as measured in the 2MASS Extended Source catalog (Skrutskie et al. 2006), with the *WISE* *W1* point spread function (PSF). This particular magnitude, called *w1gmag*, captures more light than the standard, profile-fit magnitude *w1mpro* (optimized for measuring point-sources) and is less sensitive to systematics from inclination effects. While a *w1gmag* magnitude can underestimate the true magnitude by as much as 20%¹⁰, this is a significant improvement over *w1mpro*, which typically underestimates extended source flux by 60-80%. This underestimation is encoded in the final magnitude uncertainty.

We note that alternatives to *w1gmag* are also in development (see e.g, Jarrett et al. 2012, 2013) which may provide improved magnitude estimates. In particular, an isophotal curve-of-growth analysis (combined with the careful removal of foreground stellar light) yields *W1* galaxy magnitudes that are on average 0.32 ± 0.14 mags brighter than their *w1gmag* counterparts (T. Jarrett and M. Bilicki, private communication). We can therefore revisit the issue of galaxy photometry when these alternative catalogs are released publicly. However, with a potential scatter of only ~ 0.14 mags relative to the *w1gmag* values, these updated measurements will not significantly

¹⁰ http://wise2.ipac.caltech.edu/docs/release/allsky/expsup/sec6_3e.html

affect the TF slope or dispersion parameters in our analysis (Section 3.3).

After the initial cross-matching, We begin with a set of 1929 galaxies. However, in order to improve the quality of the sample we apply a number of data cuts. Only galaxies with the highest line width quality flags (“G” from the H I archive and “A” from the HYPERLEDA data; see Springob et al. 2005 and Theureau et al. 2005, respectively for flag descriptions) are kept, as these are most accurate measurements for TF purposes. To reduce the intrinsic scatter of the line width measurement, we apply a signal-to-noise cutoff of $\sigma_{\text{width}}/\text{width} < 0.1$, and also reject galaxies with an inclination angle less than 45° . Inclination angles are derived from the axis ratio of each galaxy, but rather than measuring these quantities directly from the *WISE* catalog, we instead use the optical (V-band) axis ratios presented in the NASA/IPAC Extragalactic Database (NED)¹¹. This is done so that the axis ratio is optimized to measure the bluer disk light rather than the redder bulge light, which often underestimates ellipticity.

A morphology cut is also applied to the data, to ensure that we only select rotationally-supported galaxies in the final sample. Specifically, we select galaxies classified between type S0 (T = 0) and Sd (T = 9), using the de Vaucouleurs T-type classification scheme. Morphology information is taken from the CfA Redshift Catalog (ZCAT; Huchra et al. 2012).

After applying all cuts, we are left with 568 galaxies in the final sample. While the overall number has been dramatically reduced, the physical characteristics of the remaining galaxies are not significantly different from the original population. In particular, shapes of galaxy magnitude, line width, and recessional velocity distributions remain the same before and after the cuts are applied, and the final sample still covers a large area across the sky. Because of this, we are confident that the reduced data set is not fundamentally different from the full set, and analysis of the final galaxy sample will yield robust results.

A map of the positions of sample galaxies (in Galactic coordinates), along with a redshift distribution histogram can be seen in Figure 1. Since, as mentioned above, we do not use the 2MTF galaxy sample observed with the Parkes telescope (Hong et al. 2013), our sample is artificially cut off at -45° declination. In the lower panel, both the pre-cut (green) and post-cut (blue) redshift distributions are shown, highlighting the fact that our cuts do not significantly bias the physical properties of the galaxy sample. The observed redshift of the sample extends to 14000 km s^{-1} ($z \sim 0.045$).

3. TEMPLATE CONSTRUCTION AND ANALYSIS

Before attempting to fit a TF relation to our galaxy sample, we first apply a number of corrections to ensure homogeneity. We now briefly describe each of these corrections, and our specific methods for implementing them.

3.1. Luminosity Corrections

First, we apply several photometric corrections to the observed apparent magnitudes of the sample. In all cases,

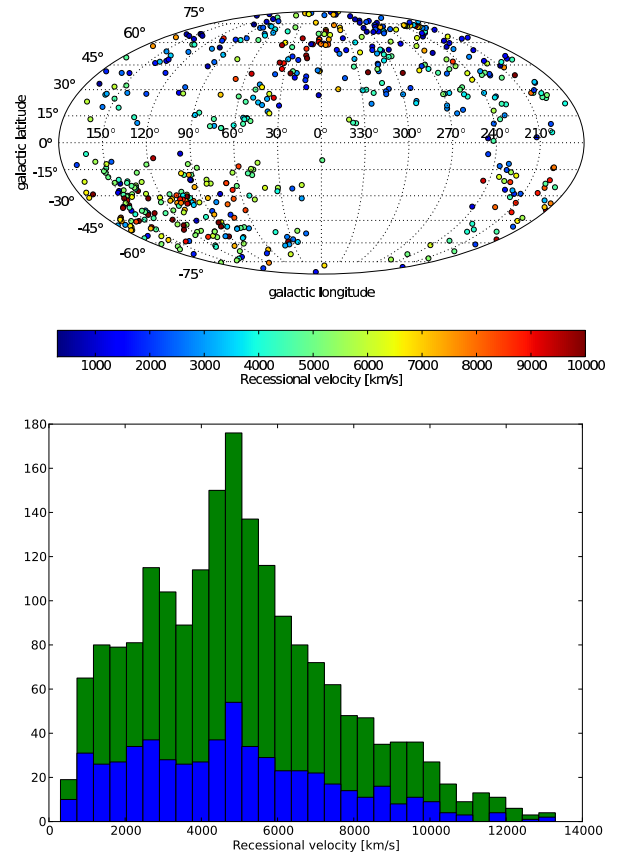


Figure 1. Coordinates and recessional velocities of the final *WISE* TF galaxy sample. **Top:** A scatterplot of galaxy coordinates, using an equal-area Mollweide projection. The data gap seen around the Equatorial South Pole is due to a lack of publicly available, calibrated 2MTF line widths. This region will be filled in as the remaining portions of the 2MTF catalog are published. The recessional velocity (redshift) of a given galaxy is indicated by color, though we apply an artificial color cutoff at $v = 10000 \text{ km s}^{-1}$ to improve the contrast of the distribution. **Bottom:** A velocity histogram showing the redshift distribution of our galaxy sample both before applying the specific cuts in Section 2 (green) and after (blue). The distribution peaks at $v = 5000 \text{ km s}^{-1}$ ($z \sim 0.015$), but galaxies continue out to $v = 14000 \text{ km s}^{-1}$ ($z \sim 0.045$).

the distance modulus required for converting a galaxy’s apparent magnitude into the absolute frame is the largest correction, but there are a number of smaller corrections necessary as well. These include adjustments for peculiar velocity (μ_H), Galactic extinction ($A_{3,6}$), and internal absorption (Δm_{Int}). We now describe each of these processes.

3.1.1. Peculiar Velocity

In the nearby Universe ($z < 0.1$), the peculiar velocity of a galaxy (i.e. additional speed and direction relative to the Hubble flow), is typically on the order of 200 km s^{-1} (Peebles 1976). Over the distance range of the *WISE* TF galaxy sample, this translates to a (cosmological) redshift uncertainty between 1.4 and 100%, giving rise to an additional 0.03 to 1.5 magnitudes of scatter in the TF relation. Removing the effects of this peculiar motion should, therefore, reduce the observed scatter. In this work, we achieve this by applying the peculiar velocity model of Erdoğan et al. (2006) to each galaxy.

Since the Erdoğan et al. (2006) model is coarsely sam-

¹¹ <http://ned.ipac.caltech.edu/>

pled, with peculiar velocity values only reported at regular (5 Mpc x 5 Mpc x 5 Mpc) intervals in Cartesian Supergalactic space, we rely on interpolation to improve the model’s utility. In particular we apply a 3rd-order, bicubic spline interpolation scheme to the model grid so that we are able to apply a unique peculiar velocity value at the coordinates of each sample galaxy. Systematic tests assessing the accuracy of our spline interpolation scheme can be seen in the Appendix.

The model provides an estimate of total velocity (v_T) as a function of Hubble flow velocity (v_H) for any supergalactic (sgl, sgb) position. We therefore interpolate over the inverse function, $v_H(v_T)$, (assuming $v_T = v_{\text{obs}} \equiv cz$, the galaxy’s observed redshift velocity) to remove the effects of peculiar velocity. The CMB reference frame is used throughout this process.

While, in general, it is not always possible to uniquely invert the total velocity function due to complications from the “triple-value problem” (see e.g., Davis & Peebles 1983; Marinoni et al. 1998), we find v_T to be monotonic with redshift for all galaxies in our sample, resulting in an unambiguous Hubble flow velocity measurement every time. The v_H values can then be used to derive a corrected distance modulus, according to the equation:

$$\mu_H = -5 \log \left[\frac{v_H}{100h} \right] - 25 \quad (1)$$

3.1.2. Extinction

In addition to peculiar velocity modifications, we also correct the *WISE* photometry for the effects of dust extinction, due to both Milky Way reddening and internal absorption from the galaxies themselves.

To correct for Galactic extinction, we apply the dust models of Schlegel et al. (1998), obtaining reddening values for each galaxy from the NASA/IRSA dust web service¹². Since the web service only offers corrections for a limited number of wavebands, we adopt the reddening correction associated with the 3.6-micron IRAC-1 channel ($A_{3.6} = 0.179 \cdot E(B - V)$), as this wavelength is the closest to that of the 3.4 micron *WISE* W1 data we use. In general, extinction due to Galactic reddening is small ($\Delta m_{\text{Gal}} < 0.05$ mag), however, the correction is still included for completeness sake.

We must also account for internal extinction by a galaxy’s interstellar medium, an effect which increases with inclination angle. For this correction, we use the same technique described in Masters et al. (2003): the modification takes the form of a broken power-law model with a shallow slope for low-to-moderate-inclination galaxies, and a steeper slope for high-inclination (nearly edge-on) galaxies. We specifically choose the broken power-law correction rather than a purely linear one (e.g., Giovanelli et al. 1994; Tully et al. 1998) to better match the redder near-IR colors of high-inclination ($\log(a/b) > 0.5$) galaxies (Masters et al. 2003). To correct the *WISE* galaxy sample, we start with the 2MTF K-band model from Masters et al. (2008), but we scale both slopes to the W1 band by a $1/\lambda$ scaling law. This serves to flatten both the low-end and high-end slopes by nearly a factor of two ($\lambda_{\text{scaling}} = 2.2\mu\text{m}/3.4\mu\text{m}$), but this

is expected, as dust absorption (both internal and external) is much less prevalent as wavelength increases. Like the Galactic extinction mentioned above, internal extinction corrections are also usually small ($\Delta m_{\text{Int}} < 0.05$ mag), though some of the steeply inclined galaxies on our sample (inclination $> 75^\circ$) can show as much as a 0.2 mag difference.

3.1.3. The full correction

After calculating all of the luminosity corrections, we apply them to the observed magnitudes, according to the equation:

$$M_{\text{corr}} = m_{\text{obs}} + \mu_H - \Delta m_{\text{Int}} - A_{3.6} \quad (2)$$

These corrected magnitudes are then used in the TF relation.

3.2. Line Width Corrections

Like the luminosity, rotation widths must also be corrected before a TF relation can be fit. In particular, we must account for systematic effects between different telescopes, line width broadening due to cosmology, turbulent motion in the disks of galaxies, and inclination of the galaxies themselves. We now briefly describe these corrections.

3.2.1. Instrumental and Cosmological Effects

Since our line width data is taken from publicly available archives, many galaxies (especially those found in the Cornell archive) have already been corrected for both instrumental and cosmological effects (see Springob et al. (2005)). If these corrections are not already available, we calculate them ourselves using other methods, according to the equation

$$W_{\text{IC}} = \frac{W_{\text{obs}} - \Delta_s}{1 + z} \quad (3)$$

where Δ_s represents the systematic instrumental correction, and the $1 + z$ term corrects for cosmological broadening.

3.2.2. Turbulent motion

Based on the turbulent motion simulations presented in Springob et al. (2005), we apply a constant correction of $\Delta_t = 6.5 \text{ km s}^{-1}$ to account for potential turbulent motion broadening. This shifts the entire TF relation to slightly lower line widths, decreasing the intercept of the fit by a small amount.

3.2.3. Galaxy Inclination

In order to further normalize our line width data, we also apply a correction for galaxy inclination. This is done using the standard $1/\sin(\theta_i)$ broadening correction, where the inclination angle θ_i is again calculated from the galaxy’s optical axis ratio.

3.2.4. The full correction

Just as before, we apply all of the above corrections to the measured line widths for the TF analysis, according to the following equation:

$$W_{\text{corr}} = \frac{W_{\text{IC}} - \Delta_t}{\sin(i)} \quad (4)$$

¹² <http://irsa.ipac.caltech.edu/applications/DUST/>

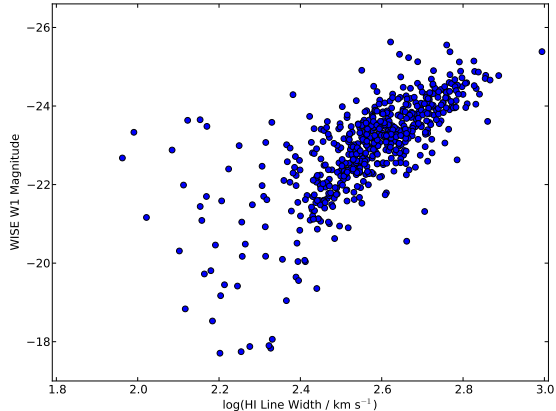


Figure 2. First look at the *WISE* 3.4 micron Tully Fisher relation, plotting total W1 magnitude against the logarithm of H I line width. We see a positive correlation between magnitude and line width, and that the dispersion on the TF relation decreases towards the bright end.

3.3. Constructing the Tully Fisher Relation

3.3.1. Initial Construction

After applying the corrections to galaxy magnitudes and line widths, we are able to create a TF relation with the data. A first look at this relation is shown in Figure 2. Like TF relations in other bands, the *WISE* TF relation shows a positive correlation between galaxy magnitude and line width, with an average dispersion that increases towards the faint end. To better quantify this behavior, we fit a line to the data, using a Levenberg-Marquardt least squares optimization routine to determine the best-fit slope and intercept parameters. The minimization itself is applied to the bivariate χ^2 function given by:

$$\chi^2 = \sum_i^N \frac{(a \cdot W_{\text{corr},i} + b - M_{\text{corr},i})^2}{(a \cdot \sigma_{W,i})^2 + (\sigma_{M,i})^2} \quad (5)$$

where a and b are the model slope and offset, respectively, W_{corr} and M_{corr} are the line widths and magnitudes of the sample galaxies, and σ_W and σ_M are the uncertainties on the measured data. These uncertainties are calculated by adding the intrinsic measurement uncertainties of the data in quadrature with the errors propagated from the corrections applied in the previous section.

To prevent outliers from biasing the results, we repeat the fitting process several times, applying a 3.5σ sigma clip to the data after each iteration. If after a particular iteration no galaxies are clipped from the sample (typically after the 3rd or 4th fit), we consider the fit to have converged and treat the final parameters as our best-fit TF slope and intercept. Examples of the fit can be seen in Figure 3.

For the initial *WISE* TF relation, we find a best-fit slope of $a = -8.13$ and a best-fit intercept of $b = 2.02$. To characterize uncertainties on the parameters, we analyze 1000 bootstrap resamplings of the data, measuring an average variation of $\sigma_a = 0.6$ and $\sigma_b = 1.8$ for the slope and intercept, respectively.

As a check on these parameters, we also fit the data with an inverse TF relation (assuming W_{corr} as the de-

pendent variable), given by

$$W_{\text{corr}} = M_{\text{corr}}/a_{\text{inv}} + b_{\text{inv}} \quad (6)$$

Like before, a_{inv} and b_{inv} are the best fit slope and intercept, respectively. To obtain the best fit, we use a modified χ^2 function:

$$\chi_{\text{inv}}^2 = \sum_i^N \frac{(M_{\text{corr},i}/a_{\text{inv}} + b_{\text{inv}} - W_{\text{corr},i})^2}{(\sigma_{W,i})^2 + (\sigma_{M,i}/a_{\text{inv}})^2} \quad (7)$$

but maintain the 3.5σ clip. The resulting best-fit parameters remain unchanged with this optimization scheme (i.e., $a_{\text{inv}} = -8.13$, $b_{\text{inv}} = 2.02$), and thus we focus only on the bivariate relation in the remaining analysis.

3.3.2. Correcting for galaxy morphology

After initially constructing *WISE* TF (Figure 2) we notice a broken power-law feature in the data, occurring at $\log(W_{\text{corr}}) = 2.6$. Giovanelli et al. (1997) and Masters et al. (2006) both found slight morphological dependencies on TF parameters, with Giovanelli et al. (1997) showing that earlier type spirals (S0 through Sb) have a slightly brighter TF intercept, and Masters et al. (2006) finding that these spirals have both brighter intercepts and intrinsically shallower slopes. It is possible, therefore, that this morphological dependence may (at least partially) explain the break that we see. To investigate this, we separate our galaxy sample (including those galaxies rejected by the sigma-clip) into three distinct morphological categories: an S0/Sa group, an Sb group, and an Sc/Sd group, and fit a separate TF relation to each set. These fits can be seen in Figure 4, and as expected, the S0/Sa and Sb galaxy samples do indeed have a shallower slope than the Sc/Sd subsample. In particular, we find slopes of $a_{S0/Sa} = -4.36$, $a_{Sb} = -7.06$, and $a_{Sc/Sd} = -9.90$. These slope discrepancies are larger than those measured by Giovanelli et al. (1997) in the optical, but are comparable to the near-IR slope discrepancies seen in the 2MTF templates (Masters et al. 2008). Furthermore, since each group occupies a distinct region of TF phase space, with the S0/Sa and Sb groups laying mainly above $\log(W_{\text{corr}}) = 2.6$ and the Sc/Sd group positioned mainly below $\log(W_{\text{corr}}) = 2.6$, the morphology dependence does appear to explain why the broken power-law feature is so distinct in Figure 2.

Following Masters et al. (2008), we apply an additional magnitude correction to S0/Sa and Sb galaxies, in order to normalize the data into a single Sc/Sd-equivalent TF relation. By doing this, we further reduce the dispersion on the *WISE* TF relation, and can more easily compare it to the 2MTF templates, which are normalized to Sc. We first fit new TF relations to the S0/Sa and Sb galaxy samples, but force the slopes to match the Sc/Sd sample slope. Differences between the Sc/Sd TF intercept and the new, fixed TF relation intercepts ($\Delta b_{S0/Sa} = 0.21$; $\Delta b_{Sb} = 0.10$) are then added to the magnitudes of a given morphological type. To correct the “tilt” of the earlier-type spirals, we also include a line-width-dependent magnitude correction, given generally by $\Delta M = \Delta a \times [\log(W) - 2.5]$, where Δa is the difference between the S0/Sa or Sb slopes and the Sc/Sd slope presented above.

After applying both the constant and line-width-dependent offsets to the S0/Sa and Sb galaxy samples,

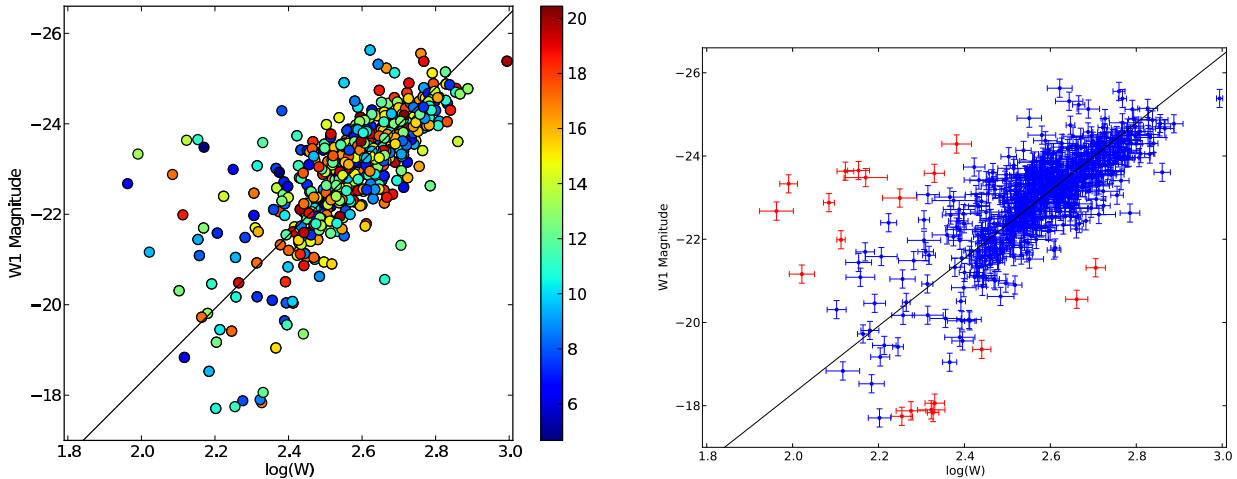


Figure 3. Best-fit TF relation (solid black line) of the *WISE* galaxy sample. Left: Best-fit line overlaid on the galaxy data. The color of a data point represents that galaxy’s specific weight in the least-squares fit. Right: Same data/TF relation overlay, but with error bars representing the relative contribution of line width and magnitude uncertainties to the error budget. In this panel, galaxies removed from the final sample by sigma clipping are indicated in red.

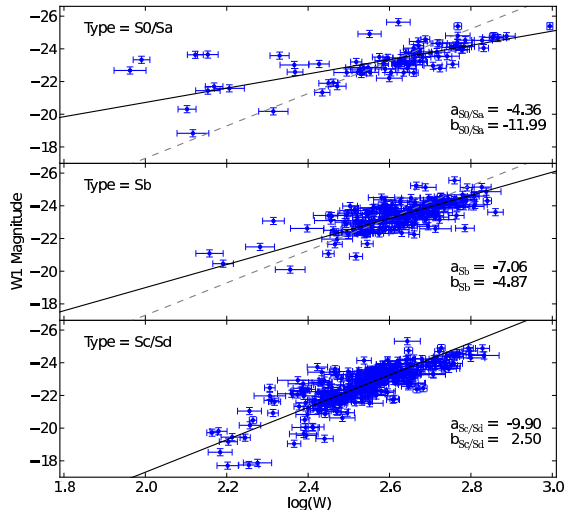


Figure 4. TF relations fit to three different morphological types: S0/Sa, Sb, and Sc/Sd. The earlier-type spiral groups clearly have a shallower TF slope. In each panel, the best-fit slope is represented by a solid black line. In the S0/Sa and Sb panels, the best fit line from the Sc/Sd morphological group is represented by a gray dashed line.

we find a secondary offset between the different morphological groups ($\Delta b_{S0/Sa, \text{new}} = 0.4$; $\Delta b_{Sb, \text{new}} = 0.20$). We therefore manually correct the galaxy magnitudes to account for these offsets, without re-fitting a TF relation. The final magnitude corrections for morphology are given by

$$\Delta M_{S0/Sa} = -0.61 - 5.54 [\log(W_{\text{corr}}) - 2.5] \quad (8)$$

$$\Delta M_{Sb} = -0.30 - 2.84 [\log(W_{\text{corr}}) - 2.5] \quad (9)$$

and the effects of these corrections can be seen in Figure 5.

With all galaxies normalized to an Sc template, we fit a new TF relation to the entire *WISE* TF galaxy sample (Figure 6), using the same bivariate fitting and sigma-clipping procedure outlined previously. The normalized relation shows a steeper overall slope ($a_{\text{TF}} = -10.05$) and fainter intercept ($b_{\text{TF}} = 2.89$) when compared to the unnormalized galaxy sample. We take these values to be our final, best-fit parameters, and use them to create a

master *WISE* TF relation:

$$M_{\text{corr}} = -22.24 - 10.05 [\log(W_{\text{corr}}) - 2.5] \quad (10)$$

The data used to construct this final relation, including the observed galaxy magnitudes and line widths, the corrections applied to the observed quantities, and final data sigma-clipping can be seen in Table 1.

To measure the total dispersion for the master *WISE* TF, we calculate the weighted standard deviation around its fitted slope. We employ an inverse variance weighting scheme, taking the total variance for a given galaxy to be the quadrature sum of the uncertainties in line width and magnitude. For our data, we find a total dispersion of $\sigma_{\text{WISE}} = 0.686$ magnitudes.

4. DISCUSSION

4.1. Comparing *WISE* TF to other TF relations

From Figure 6, it is clear that the mid-IR TF relation does not maintain the near-zero scatter presented in Figure 7d of Freedman & Madore (2010), though this is not entirely surprising. Since the sample used in Freedman & Madore (2010) is quite small (consisting of only 8 galaxies), it is possible that small-number statistics and chance alignment conspire to create the unusual result – a fact that Freedman & Madore themselves point out. By including a much larger sample of galaxies, as we have, one can gain a more complete picture of mid-IR TF magnitudes, leading to the larger dispersion estimates we see in our sample. In fact, over-plotting the Freedman & Madore (2010) sample on to the *WISE* TF relation (after adjusting the sample’s zeropoint), we find that they are perfectly consistent with many of our own galaxies (Figure 7).

The Sorce et al. (2013) mid-IR TF relation provides a better point of comparison for *WISE* TF. Also using *Spitzer* 3.6 μm photometry, Sorce et al. (2013) construct a TF relation using ~ 200 galaxies found in large clusters. While the photometric corrections they apply to their galaxies are slightly different from our own (they include small corrections for Doppler shifting and PSF diffusion, and do not include corrections for peculiar velocity or

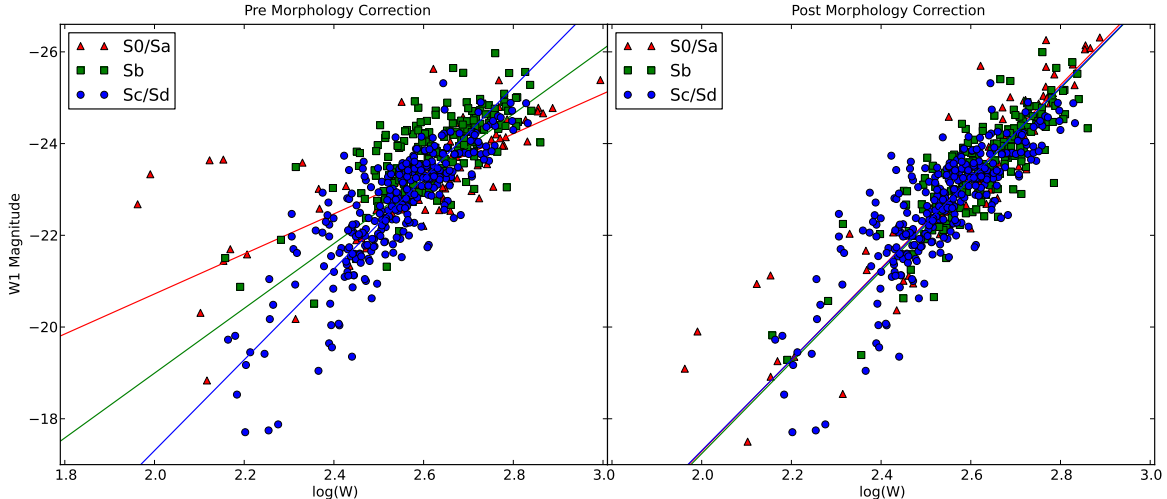


Figure 5. Effects of morphology correction on the *WISE* TF relation. **Left:** The three distinct morphological categories, S0/Sa (red triangles), Sb (green squares), and Sc/Sd (blue circles) plotted together before magnitude corrections are applied to the earlier-type groups. We note that the three groups coincide at $\log(W) = 2.6$, the location of the sharp power-law break. **Right:** The same three morphological types after applying the magnitude corrections. All galaxies are now normalized to the Sc/Sd TF relation, and can be fit together to create a “master” TF relation.

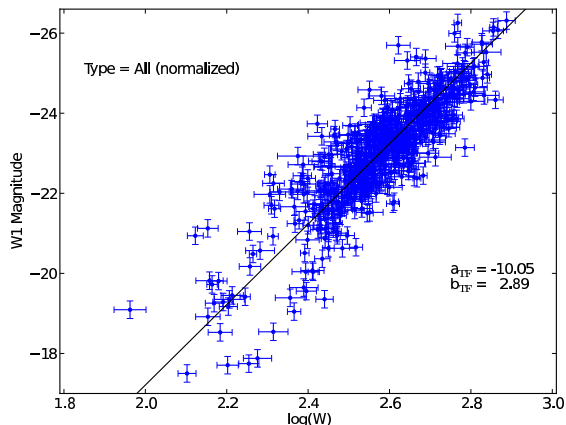


Figure 6. The *WISE* TF relation after all galaxies are normalized to an Sc/Sd morphology. While the slope of the normalized relation increases and the intercept gets dimmer, the overall dispersion of the relationship does not significantly change.

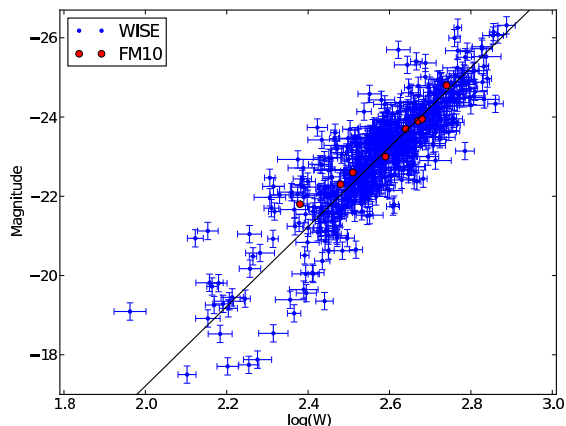


Figure 7. The Freedman & Madore (2010) TF $3.6 \mu\text{m}$ galaxy sample over-plotted on the *WISE* TF relation (after adjusting the magnitude zeropoints). The sample is fully consistent with our own set of galaxies, so it is likely a case of small-number statistics and chance alignment that gives rise to the anomalously low TF scatter.

morphology), and the analysis technique is not the same (in particular they only consider errors on line widths, rather than the bivariate fitting scheme we employ), we find that the final TF parameters agree well with *WISE* TF: $M_{3.6} = -22.84 - 9.47[\log(W_{3.6}) - 2.5]$, where the $3.6 \mu\text{m}$ zeropoint has been corrected from AB to Vega magnitudes. The total dispersion of this TF relation is $\sigma_{3.6} = 0.49$ mags, slightly lower than the value we find for *WISE* TF, but still much closer than that presented in Freedman & Madore (2010).

However, in addition to this “raw” TF relation, Sorce et al. (2013) apply an extra $(i - [3.6])$ color correction to their galaxies in order to reduce the total scatter, showing that redder galaxies tend to lie above their mean TF relation and bluer galaxies lie below (see Figure 7 in Sorce et al. 2013). This does reduce the scatter ($\sigma_{3.6,C} = 0.44$ mags) but also results in a shallower slope ($a_{3.6,C} = -9.13$). We do not apply this correction to our sample, but doing so may reduce the overall dispersion by up to 10%, based on the reduction to the $3.6 \mu\text{m}$ relation.

Since our galaxy data is drawn from the 2MTF catalog, it is also interesting to see how the *WISE* TF relation compares to the 2MTF templates. A comparison between the normalized *WISE* TF relation and the K-band 2MTF relation from Masters et al. (2008) is shown in Figure 8. For all three important TF parameters, the two relations are remarkably similar:

1. Slope: ($a_{\text{WISE}} = -10.05$, $a_{\text{K}} = -10.01$)
2. Zeropoint: ($b_{\text{WISE}} = -22.24$, $b_{\text{K}} = -22.03$)
3. Total dispersion: ($\sigma_{\text{WISE}} = 0.686$ mag, $\sigma_{\text{K}} = 0.681$ mag).

This agreement can (at least partially) be explained by examining the $(K - W1)$ colors of typical TF galaxies. In Figure 9 we show the color magnitude diagram for the galaxies in the final *WISE* TF sample. While there are a few noticeable outliers, a large majority of objects fall within 0.5 magnitudes of $(K - W1) = 0$. Of

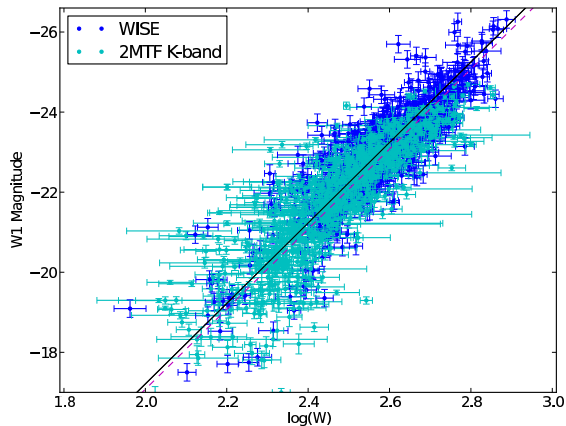


Figure 8. A comparison of the *WISE* TF relation (blue points) and the K-band 2MTF relation (cyan points) of Masters et al. (2008). The solid black line again shows the best-fit TF parameters for *WISE* TF, while the dashed magenta line shows the same for the K-band. The two relations are described by remarkably similar parameters, suggesting that both K- and W1-band observations are probing very similar stellar populations.

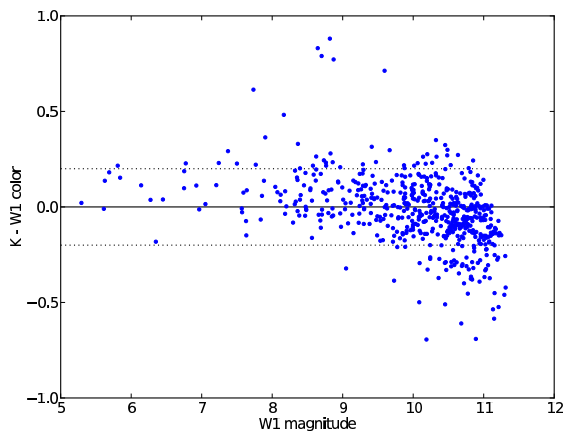


Figure 9. $K - W1$ vs. $W1$ color-magnitude diagram of the *WISE* TF galaxy sample. The $(K - W1) = 0$ color is represented by the solid line, while the dashed lines enclose $(K - W1) = \pm 0.2$. Over 80% of all *WISE* TF galaxies fall within this region, suggesting that light from the K- and W1-bands trace similar stellar populations (including older, more centrally-located stars.) It is likely that the similarity in color between the two bands helps to explain the excellent agreement between the *WISE* TF and 2MTF K-band relations.

these, nearly all are also within 0.2 magnitudes, save for a slight blueward trend at $m_{W1} \geq 10.75$. Given this near-neutral color, which suggests that the K- and W1-bands trace similar stellar populations, (including the older, centrally-located bulge stars near the cores of galaxies), it is clear the features of TF relations constructed in these two bands should very nearly mimic each other.

Like the 2MTF relations, the total scatter of the *WISE* TF relation appears to qualitatively decrease towards the bright end of the sample. Therefore, in addition to calculating a dispersion for the full data set, we also measure dispersions for subsamples of the data, binned by line width. This result is shown in Figure 10. As expected, the *WISE* TF dispersion (represented by green points) does indeed decrease as line width increases, with narrow-end galaxies showing an average dispersion of ~ 1 magnitude, and wide-end galaxies showing an average dispersion of ~ 0.5 magnitudes. Figure 10 also presents the binned K-band dispersion (red points). Comparing

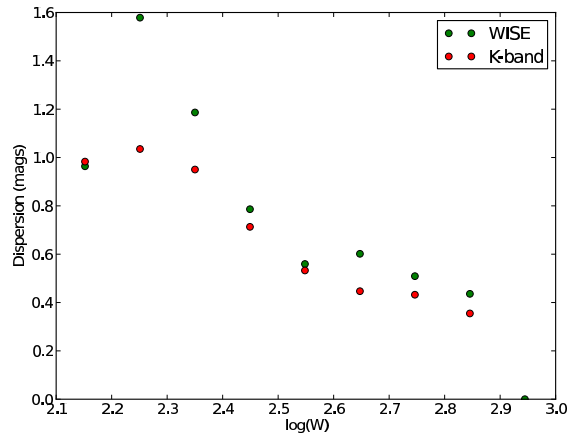


Figure 10. Average scatter of the TF relation, binned as a function of line width. We can see that the *WISE* TF relation (green points) systematically shows a larger scatter than the K-band TF relation (red points). However, both relations show an overall decrease in dispersion as line width decreases.

the two data sets, we see that the K-band relation is systematically lower than the *WISE* TF, but by $\lesssim 0.1$ magnitudes, which is within the level of statistical uncertainty.

4.2. Tully-Fisher and Bulge Light in the Mid-Infrared

Large galaxies like M31, which can compose up to 5% of a TF sample, have a prominent bulge in the mid-IR, much more so than in the optical. Assuming Model A of Widrow et al. (2003), M31-like galaxies have a bulge-to-disk luminosity ratio given by $L_R(\text{bulge})/L_R(\text{disk}) = (2.5/2.7) \times (4.4/7) = 0.58$ in the R -band. If the bulge is a magnitude redder than the disk in $(R - W1)$, the corresponding bulge-to-disk ratio in the mid-IR will instead be $L_{W1}(\text{bulge})/L_{W1}(\text{disk}) = 1.45$. This suggests that *WISE* magnitudes of the largest galaxies tend to be bulge-dominated.

In addition to the luminosity, the presence of a bulge also affects the dynamical parameter (i.e., line width) in the TF relation (Tonini et al. 2011). Switching a bulge on and off in a large galaxy, then, could perturb such a galaxy’s position in the TF relation by as much as 0.1 dex. Bulge variance in massive galaxies therefore contributes to the scatter in Tully-Fisher, and may be partially responsible for the measured dispersion in the *WISE* TF relation.

4.3. Identifying AGN contamination with *WISE* colors

Galaxies with an active nucleus (AGN) can also add to the scatter of the TF relation, as the flux coming from the active core can often dwarf the stellar emission, leading to a mismatch between a galaxy’s total magnitude and line width. Since it is possible that up to 10% of all emission-line galaxies in the Local Universe host an AGN (Brinchmann et al. 2004), it is important to identify and eliminate these objects from potential TF samples. While there are a number of successful techniques capable of identifying and segregating AGN from other galaxies, one particularly apropos method utilizes a combination of mid-IR colors (Lacy et al. 2004; Stern et al. 2005). Originally developed using the *Spitzer* IRAC wavebands, the concept has recently been extended to include *WISE* photometry, where it has been shown that a

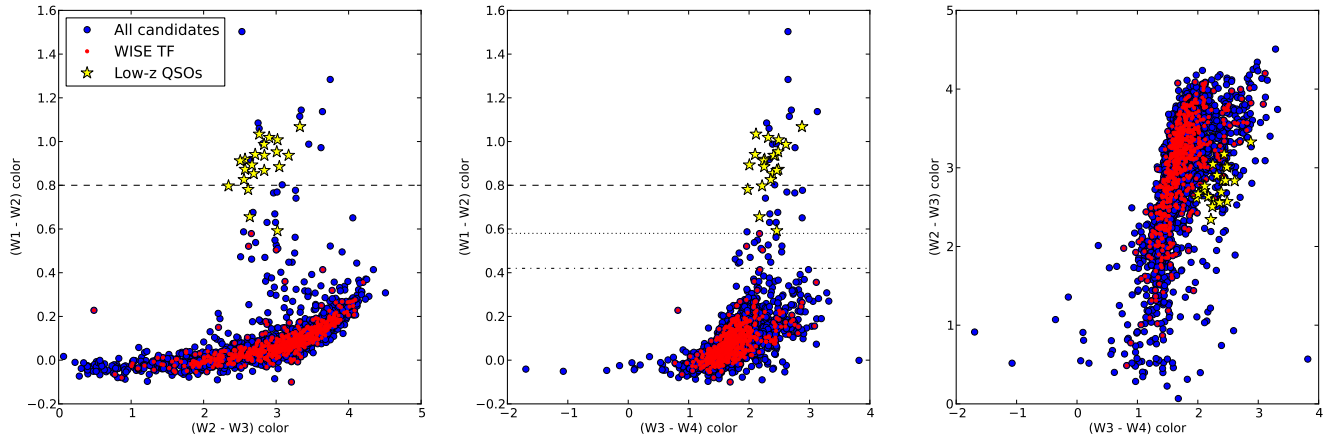


Figure 11. Various *WISE* color-color diagrams used to identify and remove Active galaxies (AGN) from normal, star-forming TF galaxies. In each panel, we plot the final *WISE* TF galaxy sample (red points), the full 2MTF candidate catalog (blue circles) and a set of known $z < 0.1$ quasars (QSOs, yellow stars). **Left:** The $(W1 - W2)/(W2 - W3)$ color space used in Yan et al. (2013). We can see a clear division between the QSOs and TF galaxies along the $(W1 - W2)$ axis, though there is a slight mixing between the QSOs and (rejected) 2MTF candidates. The $(W1 - W2 \geq 0.8)$ color cut used by Stern et al. (2012) to select AGN is shown as a dashed line. While this cut does cleanly remove many of the QSOs, some still survive, suggesting that this cut is too restrictive for our purposes. **Middle:** The $(W1 - W2)/(W3 - W4)$ color space. Here again we see the division of QSOs and normal galaxies along the $(W1 - W2)$ axis, but the overall “AGN locus” is much more prominent, largely thanks to a greatly reduced spread along the $(W3 - W4)$ axis. Along with the $(W1 - W2 > 0.8)$ line, we also plot the less restrictive $(W1 - W2 \geq 0.58)$ color cut, which just separates the reddest *WISE* TF galaxy from the bluest QSO, as a dotted line. An even bluer cut $(W1 - W2 \geq 0.42)$ that traces the very edge of the AGN locus is plotted as a dash-dotted line, but given that a few *WISE* TF galaxies are also eliminated with this cut, it may eliminate too much. **Right:** The $(W2 - W3)/(W3 - W4)$ color space. We include this panel to highlight the importance of the $(W1 - W2)$ axis, as without this color, the QSOs and normal galaxies are not nearly as well separated, providing little discriminatory power.

$(W1 - W2)$ color selection is remarkably efficient at segregating AGN from normal, star-forming galaxies – at least for objects with redshifts $z \leq 3$ (see e.g., Ashby et al. 2009; Assef et al. 2010; Eckart et al. 2010). Stern et al. (2012) and Yan et al. (2013) have further included *WISE* $W3$ - and $W4$ -band information to the detection efforts, allowing for an improved targeting of dust-obscured AGN as well.

While all of these studies share the common goal of obtaining the largest, cleanest sample of AGN, we seek to do the exact opposite – namely, determine the *WISE* color parameter(s) that will most efficiently *eliminate* AGN while keeping as many normal, star forming galaxies as possible.

In Figure 11, we plot several color-color diagrams of the *WISE* TF sample. Along with the final *WISE* TF galaxies (red points) we additionally plot the full 2MTF candidate galaxy catalog (blue circles), in order to see if there are any significant differences between “good” TF galaxies and those rejected according to other physical parameters. We also include a set of known low-redshift ($z < 0.1$) AGN (yellow stars), taken from the Wu et al. (2012) quasar (QSO) catalog, in order to better see the differences between active and normal galaxies.

In $(W1 - W2)/(W2 - W3)$ color space (left panel), we see (like previous studies) a clear separation between the QSO and TF galaxies, with the QSOs having a significantly redder $(W1 - W2)$ color. Intriguingly, the QSO color space is also populated with several rejected TF galaxy candidates, suggesting that our applied data cuts (Section 2) can at least partially eliminate some AGN contamination already. While no single cut parameter eliminates all of the galaxies above the QSO line, the line-width quality, inclination-angle, and morphology cuts are responsible for removing $\sim 80\%$ of these objects. Re-

placing the $(W2 - W3)$ color with $(W3 - W4)$ (middle panel), we still see the prominent separation between the QSOs and TF galaxies, but the overall AGN locus is much more pronounced, thanks to the reduced spread of the $(W3 - W4)$ color. In many ways the “best” dividing line between QSOs and normal galaxies is much easier to identify in this color space, and it may well be that, in the very local Universe, the $(W1 - W2)/(W3 - W4)$ parameter is an even more efficient AGN/TF discriminator. For the 2MTF catalog, cutting galaxies with $(W1 - W2) > 0.58$ should cleanly remove bright AGN without significantly impacting the galaxy sample. Finally, to highlight the importance of the $(W1 - W2)$ color, we also plot objects in $(W2 - W3)/(W3 - W4)$ color space (right panel). Unlike previous color spaces, this space does not significantly differentiate between AGN and normal galaxies, severely limiting its usefulness as a TF galaxy discriminator.

5. CONCLUSIONS

We have presented a mid-infrared extension of the Tully-Fisher relation, using luminosities obtained from the *WISE* satellite. The galaxies used in this work are taken from the all-sky, near-infrared 2MTF galaxy catalog and cover distances out to redshift $z \approx 0.045$. Prior to constructing the full TF relation, we apply a number of corrections to both the magnitudes and line widths of these galaxies, in order to reduce the observed TF scatter and better compare our results to previous work. In particular we pay special attention to correcting the effects of peculiar velocities, using the model of Erdoğan et al. (2006), and we also apply a morphology correction in order to normalize magnitudes to an Sc-type template.

After applying the corrections, we use a bivariate, least squares fitting routine to generate the best-fit TF parameters, finding a slope of $a_{\text{TF}} = -10.05$ and an intercept

of $b_{\text{TF}} = 2.89$. Transforming the line widths into a magnitude measurement leads to the final *WISE* TF relation, given by:

$$M_{\text{corr}} = -22.24 - 10.05[\log(W_{\text{corr}}) - 2.5] \quad (11)$$

We calculate the dispersion around the best fit model, measuring an average *WISE* TF scatter of $\sigma_{\text{WISE}} = 0.686$. However, we find that the overall scatter is strongly dependent on line width, with galaxies near $\log(W_{\text{corr}}) = 2.3$ having a dispersion approximately 0.5 mags greater than galaxies near $\log(W_{\text{corr}}) = 2.9$.

We find that the *WISE* TF relation is significantly different from the preliminary $3.6 \mu\text{m}$ *Spitzer* TF relation presented in Freedman & Madore (2010), with *WISE* TF having both a steeper slope and larger scatter. This is not surprising, however, given the small sample size and unusually bright galaxies chosen in that work. Conversely, we find good agreement between *WISE* TF and the cluster-based mid-IR TF relation presented in Sorce et al. (2013). Given these similarities, in spite of somewhat different analytical techniques, we conclude that a steeper, more scattered TF relation better describes the properties of galaxies observed in the mid-IR than the optimistic results of Freedman & Madore (2010).

Finally, we also compare *WISE* TF to the near-IR (*K*-band) 2MTF template relation presented in Masters et al. (2008), and find that, both in terms of TF parameters and in total dispersion, the two relations agree extremely well, with both showing a TF slope near the theoretical limit of $L \propto v_{\text{rot}}^4$ predicted from physical arguments. This result may not be entirely surprising, given that the typical (*K* – *W1*) color of *WISE* TF galaxies is ~ 0 , and it suggests that the *K*-band and *W1*-bands are tracing similar stellar populations (including the older, centrally-located stars in the bulge). Whether this agreement holds for TF relations constructed at longer wavelengths – where the observed light from thermally-heated dust will ostensibly begin to trace the younger, disk-dominated stars again – is unknown, but would be an interesting question to examine in future work.

The authors wish to thank the anonymous referee for thoroughly reading this manuscript and for providing several helpful comments and suggestions that greatly improved the work. We also thank Pirin Erdođdu for providing the initial peculiar velocity model. This research was conducted by the Australian Research Council Centre of Excellence for All-sky Astrophysics (CAASTRO), through project number CE110001020. This publication makes use of data products from the Wide-field Infrared Survey Explorer, which is a joint project of the University of California, Los Angeles, and the Jet Propulsion Laboratory/California Institute of Technology, funded by the National Aeronautics and Space Administration. This research has made use of the NASA/IPAC Extragalactic Database (NED) which is operated by the Jet Propulsion Laboratory, California Institute of Technology, under contract with the National Aeronautics and Space Administration.

REFERENCES

- Aaronson, M., Huchra, J., & Mould, J. 1979, *ApJ*, 229, 1
 Aaronson, M., Mould, J., & Huchra, J. 1980, *ApJ*, 237, 655
 Ashby, M. L. N., Stern, D., Brodwin, M., et al. 2009, *ApJ*, 701, 428
 Assef, R. J., Kochanek, C. S., Brodwin, M., et al. 2010, *ApJ*, 713, 970
 Bernstein, G. M., Guhathakurta, P., Raychaudhury, S., et al. 1994, *AJ*, 107, 1962
 Bothun, G. D., & Mould, J. R. 1987, *ApJ*, 313, 629
 Brinchmann, J., Charlot, S., White, S. D. M., et al. 2004, *MNRAS*, 351, 1151
 Buta, R. J., Sheth, K., Regan, M., et al. 2010, *ApJS*, 190, 147
 Dale, D. A., Gil de Paz, A., Gordon, K. D., et al. 2007, *ApJ*, 655, 863
 Davis, M., & Peebles, P. J. E. 1983, *ARA&A*, 21, 109
 Djorgovski, S., & Davis, M. 1987, *ApJ*, 313, 59
 Dressler, A. 1987, *ApJ*, 317, 1
 Dressler, A., Lynden-Bell, D., Burstein, D., et al. 1987, *ApJ*, 313, 42
 Eckart, M. E., McGreer, I. D., Stern, D., Harrison, F. A., & Helfand, D. J. 2010, *ApJ*, 708, 584
 Erdođdu, P., Lahav, O., Huchra, J. P., et al. 2006, *MNRAS*, 373, 45
 Faber, S. M., & Jackson, R. E. 1976, *ApJ*, 204, 668
 Ferrarese, L., & Merritt, D. 2000, *ApJ*, 539, L9
 Freedman, W. L., & Madore, B. F. 2010, *ARA&A*, 48, 673
 Giovanelli, R., Haynes, M. P., Salzer, J. J., et al. 1994, *AJ*, 107, 2036
 Giovanelli, R., Haynes, M. P., Herter, T., et al. 1997, *AJ*, 113, 53
 Hong, T., Staveley-Smith, L., Masters, K. L., et al. 2013, arXiv:1304.0882
 Huchra, J. P., Macri, L. M., Masters, K. L., et al. 2012, *ApJS*, 199, 26
 Jarrett, T. H., Masci, F., Tsai, C. W., et al. 2012, *AJ*, 144, 68
 Jarrett, T. H., Masci, F., Tsai, C. W., et al. 2013, *AJ*, 145, 6
 Lacy, M., Storrie-Lombardi, L. J., Sajina, A., et al. 2004, *ApJS*, 154, 166
 Macri, L. M. 2001, Ph.D. Thesis,
 Masters, K. L., Giovanelli, R., & Haynes, M. P. 2003, *AJ*, 126, 158
 Masters, K. L., Springob, C. M., Haynes, M. P., & Giovanelli, R. 2006, *ApJ*, 653, 861
 Masters, K. L., Springob, C. M., & Huchra, J. P. 2008, *AJ*, 135, 1738
 Marinoni, C., Monaco, P., Giuricin, G., & Costantini, B. 1998, *ApJ*, 505, 484
 Mocz, P., Green, A., Malacari, M., & Glazebrook, K. 2012, *MNRAS*, 425, 296
 Patrel, G., Theureau, G., Bottinelli, L., et al. 2003, *A&A*, 412, 57
 Peebles, P. J. E. 1976, *Ap&SS*, 45, 3
 Pérez, E., Cid Fernandes, R., González Delgado, R. M., et al. 2013, *ApJ*, 764, L1
 Rothberg, B., Saunders, W., Tully, R. B., & Witchalls, P. L. 2000, *ApJ*, 533, 781
 Sakai, S., Mould, J. R., Hughes, S. M. G., et al. 2000, *ApJ*, 529, 698
 Schlegel, D. J., Finkbeiner, D. P., & Davis, M. 1998, *ApJ*, 500, 525
 Skrutskie, M. F., Cutri, R. M., Stiening, R., et al. 2006, *AJ*, 131, 1163
 Sorce, J. G., Courtois, H. M., & Tully, R. B. 2012, *AJ*, 144, 133
 Sorce, J. G., Tully, R. B., & Courtois, H. M. 2012, *ApJ*, 758, L12
 Sorce, J. G., Courtois, H. M., Tully, R. B., et al. 2013, *ApJ*, 765, 94
 Springob, C. M., Haynes, M. P., Giovanelli, R., & Kent, B. R. 2005, *ApJS*, 160, 149
 Stern, D., Eisenhardt, P., Gorjian, V., et al. 2005, *ApJ*, 631, 163
 Stern, D., Assef, R. J., Benford, D. J., et al. 2012, *ApJ*, 753, 30
 Theureau, G., Bottinelli, L., Coudreau-Durand, N., et al. 1998, *A&AS*, 130, 333
 Theureau, G., Coudreau, N., Hallet, N., et al. 2005, *A&A*, 430, 373
 Theureau, G., Hanski, M. O., Coudreau, N., Hallet, N., & Martin, J.-M. 2007, *A&A*, 465, 71
 Tonini, C., Maraston, C., Ziegler, B., et al. 2011, *MNRAS*, 415, 811
 Tully, R. B., & Fisher, J. R. 1977, *A&A*, 54, 661

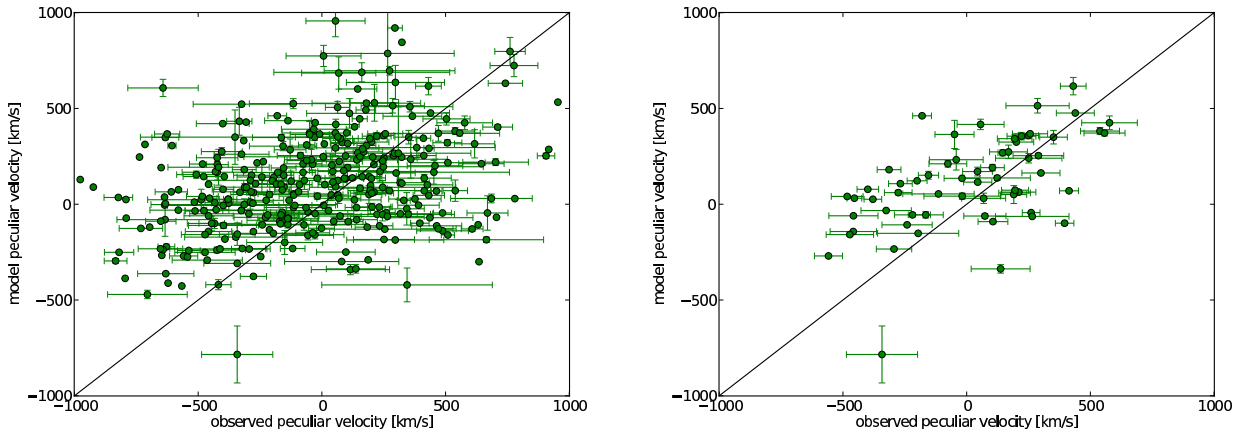


Figure 12. Comparisons between observed and model peculiar velocities, using galaxies with known redshift-independent distance measurements. **Left:** All galaxies with Type-Ia supernova distance measurements from the on-line NED-D database, within a 247.5 Mpc radius of the Earth. **Right:** Only those galaxies in the database with at least 10 independent distance measurements. In both panels, any galaxy with multiple distance measurements is represented by a single (averaged) data point, with error bars representing the dispersions on the measurements.

Tully, R. B., & Pierce, M. J. 2000, ApJ, 533, 744
 Tully, R. B., Pierce, M. J., Huang, J.-S., et al. 1998, AJ, 115, 2264
 Verheijen, M. A. W. 2001, ApJ, 563, 694
 Widrow, L. M., Perrett, K. M., & Suyu, S. H. 2003, ApJ, 588, 311
 Wright, E. L., Eisenhardt, P. R. M., Mainzer, A. K., et al. 2010, AJ, 140, 1868

Wu, X.-B., Hao, G., Jia, Z., Zhang, Y., & Peng, N. 2012, AJ, 144, 49
 Yan, L., Donoso, E., Tsai, C.-W., et al. 2013, AJ, 145, 55
 Zheng, X. Z., Dole, H., Bell, E. F., et al. 2007, ApJ, 670, 301

APPENDIX

TESTING THE ACCURACY OF THE PECULIAR VELOCITY INTERPOLATION

While the interpolation procedure we use to smooth the Erdoğdu et al. (2006) peculiar velocity model allows us to select a more diverse range of peculiar velocities, these values may not always be correct, especially if the real velocity field varies in an unexpected way between data points. Inaccurate velocity corrections can cause problems in the analysis, fundamentally change the fitted TF parameters, or at the very least increase the overall TF dispersion, leading to a pessimistic assessment of *WISE* magnitudes for TF purposes. Therefore, to check the accuracy of our interpolation scheme we compare our model peculiar velocities to real data, using galaxies with known redshifts and (redshift-independent) distances.

To collect a sample of galaxies with known distances, we turn to the NED-D database¹³, an online compilation of redshift-independent distance measurements taken from the literature. While the full NED-D catalog contains over 60000 measurements, we limit our selection to distances calculated from Type-Ia supernova data, and further limit this subsample to galaxies located less than 247.5 Mpc away from the Earth (the limit of the Erdoğdu et al. 2006 model). This leaves us with a total of 2189 measurements for 373 unique galaxies.

We calculate peculiar velocities from these data using the standard technique of combining the distance measurement (D_{obs}) with its assumed Hubble constant (H_0 , also provided from NED-D) and redshift (z_{obs}), according to:

$$v_{\text{pec, obs}} = c \cdot z_{\text{obs}} - H_0 \cdot D_{\text{obs}} \equiv v_{\text{T, obs}} - v_{\text{H, obs}} \quad (\text{A1})$$

where v_{T} and v_{H} are, respectively, the total and Hubble flow recessional velocities mentioned in Section 3.1.1.

For each observed peculiar velocity, we also generate a corresponding model value using our interpolation method. Since we already know the distances to these objects (and hence, their true position in model space), we do not need to iterate over the total velocity field like we did for the galaxies in the main TF sample (Section 3.1.1) to measure a model peculiar velocity. Instead, the peculiar velocity can be measured directly, using an object's supergalactic coordinates and observed distance:

$$v_{\text{pec, mod}} = v_{\text{P}}(\text{sgl}, \text{sgb}, D_{\text{obs}}) \quad (\text{A2})$$

where v_{P} is simply the Erdoğdu et al. (2006) model without a Hubble flow component.

The comparison between observed and model peculiar velocity values is presented in Figure 12. The left panel of the figure shows all galaxies taken from the NED-D catalog, while the right panel shows only those galaxies which have at least 10 independent distance measurements. In both panels (for the sake of clarity) we average all measurements of a given galaxy into a single data point, using error bars to represent the dispersion of both quantities.

Overall, a meaningful description of the differences between the observed and model peculiar velocities is difficult, especially given that the error bars on the observed velocities are large. While the full galaxy sample shows a mild positive correlation between the two quantities ($\rho_{\text{(full)}} = 0.30$), there is still a significant dispersion around the 1:1 correspondence line ($\sigma_{\text{(full)}} = 350 \text{ km s}^{-1}$). However, the correlation increases ($\rho_{\text{(m>10)}} = 0.57$) and the dispersion

¹³ <http://ned.ipac.caltech.edu/Library/Distances/>

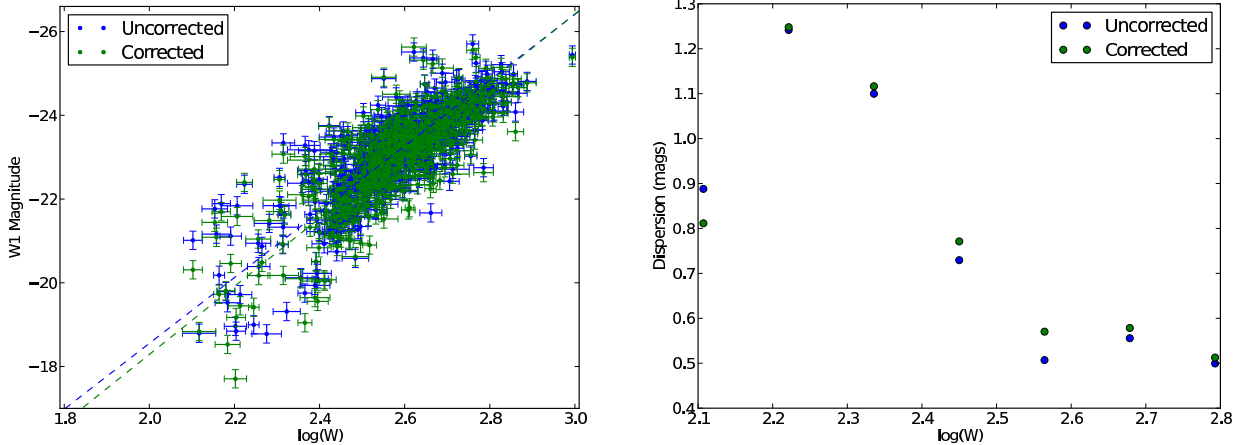


Figure 13. Effects of the peculiar velocity correction on the *WISE* TF relation. **Left:** The full galaxy sample and best-fit TF lines. **Right:** Measured dispersion around the best-fit TF parameters. In both the overall appearance and total dispersion the peculiar-velocity corrected TF relation (green) does not significantly deviate from the uncorrected (blue) relation.

decreases ($\sigma_{(m>10)} = 300 \text{ km s}^{-1}$) when focusing only on the galaxies with 10 or more distance measurements, suggesting that, at least in cases where the distance to a galaxy is well constrained, there is not as significant a disagreement between observation and our model.

Given the moderate success in recreating observed peculiar velocities, then, we believe that our interpolated peculiar velocity model will not statistically bias the magnitudes of our galaxy sample, and can thus be safely used to construct the *WISE* TF relation.

MEASURING THE EFFECTS OF THE PECULIAR VELOCITY MODEL

To observe the effects of peculiar velocity on the TF relation, we rerun the analysis without applying the interpolated model, then compare the parameters of this new TF model to the original. This is done after applying the initial magnitude and line width corrections (Section 3.3.1), but *before* applying the morphology correction (Section 3.3.2). Figure 13 shows the results of this comparison, both in terms of the fit parameters (left panel) and total dispersion (right panel). Overall, we find that the peculiar velocity correction does not significantly alter the final results. While the slope of the uncorrected relation is nominally shallower ($a_{\text{uncorr}} = -7.86$), the intercept is brighter ($b_{\text{uncorr}} = -2.83$) and the dispersion measurements differ (the corrected relation shows slightly lower dispersions at the narrow line width end and slightly higher dispersions at the wide end), all of these changes are well within the current limits of statistical uncertainty. This is not entirely unexpected, given that on average a peculiar velocity correction alters galaxy magnitudes by less than 0.2 magnitudes, while the measured dispersion of the overall *WISE* TF relation ranges between 0.5 and 1.5 magnitudes (Figure 10).

This suggests that peculiar velocities do not contribute significantly to the dispersion budget of the TF relation (at least when dealing with mid-IR magnitudes), and that the scatter is instead driven by some other, unidentified parameter. However, even though the total effect is small, we still choose to include the peculiar velocity correction in our analysis, for the sake of completeness.

Table 1
Tully-Fisher Data.

Galaxy Name (1)	RA (2)	Dec (3)	θ_i (4)	T-Type (5)	v_{obs} (6)	v_{H} (7)	m_{obs} (8)	μ_{H} (9)	m_{Int} (10)	$A_{3,6}$ (11)	ΔM (12)	M_{corr} (13)	M_{err} (14)	W_{IC} (15)	W_{corr} (16)	W_{err} (17)	clip (18)
UGC 00005	0.773583	-1.913798	60.9	4	7288	7384	10.167	-34.341	0.008	0.051	0.000	-24.233	0.218	461	520	23	N
NGC 7814	0.812280	16.145229	68.0	2	1051	1063	7.053	-30.132	0.009	0.064	0.239	-23.391	0.217	460	489	9	N
UGC 00014	0.895900	23.200779	46.8	4	7254	7206	10.767	-34.289	0.019	0.027	0.000	-23.567	0.219	332	446	34	N
UGC 00039	1.392929	53.631325	60.9	5	9523	9513	10.606	-34.892	0.082	0.051	0.000	-24.418	0.218	496	560	23	N
UGC 00040	1.451719	27.449430	51.9	3	7526	7602	10.960	-34.405	0.014	0.033	0.140	-23.632	0.218	362	452	26	N
UGC 00051	1.668191	5.113459	48.7	4	5371	5078	11.306	-33.529	0.006	0.030	0.000	-22.258	0.219	280	364	24	N
NGC 0002	1.821281	27.678375	54.7	2	7547	7637	11.070	-34.415	0.013	0.037	0.032	-23.426	0.218	344	413	19	N
NGC 0010	2.143900	-33.858337	60.9	6	6804	6515	9.236	-34.070	0.002	0.051	0.000	-24.887	0.217	550	622	17	N
NGC 0023	2.472548	25.923786	53.3	1	4565	4164	8.689	-33.098	0.007	0.035	0.337	-24.788	0.218	382	468	24	N
NGC 0019	2.670312	32.983078	60.9	4	4788	4316	10.512	-33.175	0.008	0.051	0.000	-22.722	0.218	302	338	10	N

Identifying features and physical parameters for each galaxy in the master *WISE* TF relation. In column 1, we present the galaxy's preferred common name, as displayed in NED. Columns 2 and 3 show galaxy coordinates in decimal degrees. The inclination angle (also in degrees) is shown in column 4. Galaxy morphology is presented in column 5, in the form of the de Vaucouleurs T-type classification scheme. The observed and Hubble-flow recession velocities (in km s^{-1}), are displayed in columns 6 and 7, respectively. The observed, apparent *WISE* W1 magnitude is presented in column 8, and the distance modulus is presented in column 9. Corrections to the observed galaxy magnitude are displayed in columns 10 through 12, with column 10 showing the correction for internal extinction, column 11 showing the correction for Galactic extinction, and column 12 showing any morphology-based corrections, normalizing all galaxies to type Sc ($T = 5$). The final, fully corrected absolute magnitude is presented in column 13, and its error is shown in column 14. The observed (instrument-corrected) line width (in km s^{-1}) is shown in column 15, while the fully-corrected line width is presented in column 16, along with its uncertainty in column 17. Finally column 18 shows the sigma-clipping flag for each galaxy, with 'N' meaning the galaxy is included in the final TF fit, and 'Y' meaning the galaxy is removed prior to the final fit.

Table 1 is published in its entirety in the electronic edition of *The Astrophysical Journal*. A portion is shown here for guidance regarding its form and content.